HHS Public Access

Author manuscript

Nat Cell Biol. Author manuscript; available in PMC 2013 August 01.

Published in final edited form as:

Nat Cell Biol. 2013 February ; 15(2): 169–178. doi:10.1038/ncb2647.

Rab10 GTPase regulates ER dynamics and morphology

Amber R. English[1] and **Gia K. Voeltz**[1,*]

[1]Department of Molecular, Cellular and Developmental Biology, University of Colorado, Boulder, CO 80309, USA

Abstract

We have identified Rab10 as an ER specific Rab GTPase that regulates ER structure and dynamics. We show that Rab10 localizes to the ER and to dynamic ER-associated structures that track along microtubules and mark the position of new ER tubule growth. Rab10 depletion or expression of a Rab10 GDP-locked mutant alters ER morphology, resulting in decreased ER tubules. We demonstrate that this defect is due to a reduced ability of dynamic ER tubules to grow out and successfully fuse with adjacent ER. Consistent with this function, Rab10 partitions to dynamic ER-associated domains found at the leading edge of almost half of all ER tubule dynamics. Interestingly, this Rab10 domain is highly enriched with at least two ER enzymes that regulate phospholipid synthesis, PI Synthase and CEPT1. Both the formation and function of this Rab10/PIS/CEPT1 dynamic domain is inhibited by expression of a GDP-locked Rab10 mutant. Together, these data demonstrate that Rab10 regulates ER dynamics and further suggests that these dynamics could be coupled to phospholipid synthesis.

The Endoplasmic Reticulum (ER) is a large membrane bound compartment composed of multiple structurally distinct domains spread throughout the cytoplasm of eukaryotic cells. A particularly striking feature of the ER is its extremely dynamic nature and ability to maintain its continuity during rearrangements of its complex morphology. In recent years, some of the factors that regulate ER dynamics have been identified. In animal cells, ER tubules are generated when they are pulled along microtubules (MTs) and contact an adjacent ER region where it subsequently undergoes a homotypic fusion reaction[1–4]. This homotypic fusion reaction results in the formation of a 3-way junction, which produces the reticular peripheral ER morphology. Homotypic ER fusion has been shown to be regulated by the Atlastin family of dynamin-like GTPases[5–7]. It is not known what regulates the growth and tethering between ER tubules and molecular motors on MTs during dynamics and fusion.

Numerous membrane compartments derive functional specificity from the precise combination of Rab proteins and SNAREs that guide fusion between donor and acceptor compartments[8–10]. These GTP binding proteins regulate the fusion of donor and target membranes in a process regulated by GTP hydrolysis[11, 12]. *In vitro* systems for ER formation suggest that a Rab GTPase could also regulate ER fusion[13, 14]. Here we identify

*Contact: gia.voeltz@colorado.edu.

Rab10 as an ER-specific Rab GTPase that regulates ER tubule extension and fusion at the leading edge of ER dynamics.

RESULTS

A Rab GTPase is required for ER assembly *in vitro*

Based on previous data implicating a Rab GTPase in ER assembly[13, 14], we aimed to isolate Rab proteins localized to ER membranes. We started with ER vesicles isolated from unfertilized *Xenopus laevis* egg extracts[15, 16]. These ER vesicles fuse to form a tubular ER network in the presence of hydrolyzable GTP (Fig. 1a), as previously described[15, 16]. We tested if pre-incubation of ER vesicles with recombinant Rab GDI would be inhibitory. Indeed, Rab GDI pre-incubation inhibits *in vitro* ER fusion and tubule formation (Fig. 1a, bottom middle panel), similar to previously published reports[13, 14]. Rab GDI also inhibits ER formation when assayed quantitatively using a previously described Ca^{2+} release assay (Fig. 1b)[16]. These results demonstrate that our *in vitro* ER network formation assay is sensitive to Rab GDI addition and is likely to require a Rab protein.

To identify a Rab protein tightly associated with *Xenopus* ER membranes, we optimized a purification scheme utilizing the GTP-binding ability of Rab proteins (Fig. 1c)[11, 12]. ER vesicles were washed with a non-inhibitory buffer containing 500 mM KCl to remove cytosolic or loosely associated proteins (Fig. 1a, bottom right panel). Washed vesicles were solubilized with 1% Digitonin and applied to a GTP-agarose column. A control sample was alternatively pre-incubated with 1 mM GTPγS to pre-block GTP-binding sites prior to GTP-agarose binding. The GTP-binding proteins were eluted from the column with GTP, and analyzed by SDS-PAGE (Fig. 1d). The unique ~25 kDa and ~45 kDa bands were excised and analyzed by mass spectrometry. The ~45 kDa band was identified as tubulin and the ~25 kDa band included several Rab proteins represented to different degrees of sequence coverage: Rab11 (40%), Rab8/10 (29%), Rab7 (20%), Rab2 (18%), and Rab1 (17%).

We tested if Rab proteins are displaced from ER vesicles by concentrations of Rab GDI that inhibit ER formation. ER vesicles were incubated with increasing concentrations of Rab GDI and pelleted to separate soluble and membrane fractions. Fractions were subjected to SDS-PAGE and immuno-blot analysis with an antibody recognizing *Xenopus laevis* Rab8/10 (Fig. 1e). Pre-incubation with Rab GDI caused Rab8/10 to be displaced from the membrane into the soluble fraction (Figure 1e). Our attempts to rescue Rab GDI-inhibited fusion by reconstitution of purified recombinant Rabs into the Rab GDI treated membranes were unsuccessful, perhaps because Rab GDI displaces multiple components of the fusion machinery. Regardless, these data support a model whereby Rab GDI inhibits ER formation by Rab displacement.

Rab10 localizes to the ER

To further characterize the identified Rab candidates, we generated fluorescently tagged human homolog expression constructs of a subset of these candidates. These Rab constructs were transiently co-transfected into Cos-7 cells with a luminal ER marker (KDEL-targeted) to determine localization of each Rab relative to the ER by live confocal fluorescence

microscopy (FM). Several Rabs previously shown to localize to endocytic compartments gave the expected localization[17–19] and did not localize to the ER membrane (including Rab5, Rab7, and Rab11, Supplementary Fig. 1a). *Xenopus laevis* Rab8/10 has two human paralogs (Rab8 and Rab10, Fig. 2a, Supplementary Fig. 2a). Despite their high sequence similarity (Supplementary Fig. 2a), Rab8 localized to vesicles (Fig. 2a top panel), consistent with its previously defined localization[20]. In contrast, Rab10 co-localized with multiple domains of the ER, including the nuclear envelope (NE) and peripheral ER cisternae and tubules (Fig. 2a, Supplementary Movie 1), even with low transfection levels (Supplementary Fig. 2b). Rab10 also localized to the Golgi (labeled with GPP130-eGFP, Supplementary Fig. 2c), consistent with previous reports[21]. Rab10 does not localize to the mitochondria, early endosomes or recycling endosomes (Supplementary Fig. 2c). While previous studies have not assayed if Rab10 co-localizes with ER markers, images of Rab10 in *C. elegans* reveals a reticular structure reminiscent of tubular ER[22, 23].

Rab10 regulates ER morphology

The mechanisms that regulate the Rab family of GTPases are well known and GTP-binding state mutations can be engineered to alter the activity of Rab proteins[24]. We generated two mutants of Rab10: a GTP-locked Q68L mutation and a GDP-locked T23N mutation. In both Cos-7 (Fig. 2b) and HeLa cells (Supplementary Fig. 3a), the fluorescently tagged wild type (WT) and mutant Rab10 proteins are localized to the ER (although mCh-Rab10 T23N is also cytosolic). Immuno-blot analysis shows transfected cells express 2–3 fold more fusion protein relative to endogenous Rab10 (Supplementary Fig. 3b). Confocal FM reveals that the expression of mCh-Rab10 T23N mutant alters peripheral ER shape, resulting in more cisternal regions and less tubules (compared to mCh-Rab10 WT or controls, Fig. 2a, b). We developed a quantitative assay to measure the effect of Rab10 T23N expression on ER morphology by determining the ratio of cisternae to tubules (as described in the Online Methods, Fig. 2c). The peripheral ER was 23% cisternal in control cells expressing KDEL-venus alone (Fig. 2d). Cells co-transfected with KDEL-venus and mCh-Rab10 WT or mCh-Rab10 Q68L were similar (19% and 21% cisternae, respectively, Fig. 2d). In contrast, cells expressing KDEL-venus and mCh-Rab10 T23N had a statistically significant increase in the percent of cisternae (52%, Fig. 2d). The effect of mCh-Rab10 T23N expression on ER shape is intermediate in magnitude to overexpressing Climp63 (80% cisternal, Supplementary Fig. 4c, d), an ER protein known to proliferate cisternal ER[25].

We next tested the effect of Rab10 depletion on peripheral ER shape. Cells were co-transfected with control or Rab10 siRNA together with an ER marker (KDEL-venus) to visualize shape (Fig. 3a). Rab10 siRNA treatment led to a noticeable expansion of cisternal ER and a reduction of ER tubules (Fig. 3a). Immuno-blot analysis confirmed Rab10 depletion (Fig. 3b). We quantified the effect of Rab10 depletion on peripheral ER shape as before. Rab10 siRNA-treated cells had a significant increase in cisternal ER relative to the control (68% versus 25%, respectively, Fig. 3a, c). We did not observe an effect of Rab10 depletion on Golgi morphology, even though Rab10 also localizes to Golgi (Supplementary Fig. 4a).

Rab10 alters the efficiency of ER tubule extension and fusion

Rab10 depletion or Rab10 T23N expression lead to an increase in ER cisternae; this phenotype is similar to when ER tubule-shaping proteins, reticulons, are depleted[16, 26] or MTs are depolymerized[2]. Thus, Rab10 may play a role in maintaining and/or generating the structure of ER tubules. We next tested if Rab10 regulates ER tubule extension and fusion. Using live, time-lapse FM images of Cos-7 cells transfected with KDEL-venus alone, and mCh-Rab10 WT or mCh-Rab10 T23N, we measured the number of ER tubule extension events occurring within a 10 μm^2 box over a 5 minute time period and determined if the extended tubules could successfully fuse. Fusion was "successful" if an ER tubule grew out, contacted the adjacent ER, and generated a 3-way junction maintained for more than 30 seconds (Fig. 4a, top panel). An "unsuccessful" event was when an ER tubule extended into another section of the ER but did not successfully fuse (Figure 4a, bottom panel). Cells expressing KDEL-venus alone or co-transfected with mCh-Rab10 WT had similar successful fusion rates of 74% (mean of 9.5 out of 12.9 events) and 79% (mean of 10.2 out of 13.0 events), respectively (Fig. 4b, c). In contrast, cells expressing KDEL-venus with mCh-Rab10 T23N had a reduced rate of both successful fusion and extension (51%, 5.5 out of 10.7 events, Fig. 4b, c). We observed a similar change when we instead normalize events relative to the total area of ER in the 10 μm^2 box (Supplementary Fig. 5a).

We also tested the effect of Rab10 depletion on ER tubule extension and fusion efficiency. Cells were co-transfected with KDEL-venus and either control siRNA or Rab10 siRNA (Fig. 4d). Control cells had a successful fusion rate of 79% (mean of 9.2 out of 11.9 events) compared to 53% (mean of 5.7 out of 10.6 events) for Rab10-depleted cells (Fig. 4e, f). We observed a similar change when we instead normalize the events relative to the total area of ER in the 10 μm^2 box (Supplementary Fig. 5b). Thus, Rab10 depletion or Rab10 T23N expression reduces the efficiency of ER tubule extension and fusion, explaining how the loss of functional Rab10 results in depleted tubular ER morphology.

A Rab10/PIS dynamic domain leads ER tubule extension and fusion

Live-cell imaging reveals Rab10 structures localized not only to the ER, but also to dynamic ER-associated domains (Fig. 2a and Supplementary Movie 1). Time-lapse images of these Rab10 dynamic domains relative to a general ER marker show that they precede the path of new ER tubule growth (Fig. 5a). In animal cells, most ER dynamics are dependent on the MT network[2, 3]. We asked if these Rab10-dynamic domains track along MTs by imaging cells co-transfected with BFP-Rab10, mCh-α-tubulin, and an ER marker (Supplementary Fig. 6a). BFP-Rab10 localized to the ER network and to dynamic domains tracking along MTs (Supplementary Fig. 6a)[27]. To depolymerize MTs, we treated cells with nocodazole (NZ, 5 μM) for 60 minutes[3, 27], and measured if Rab10-mediated dynamics were reduced. We performed overlays of ER images taken 1 minute apart at three time points: before, 20 min post, and 60 min post NZ treatment (Supplementary Fig. 6b). These overlays reflect the extent to which the ER network and Rab10 dynamic domains move during a 1 min time period. Rab10 dynamic domains stop moving by 60 min post NZ treatment, when virtually all MTs are depolymerized. These data demonstrate that Rab10 dynamics depend on MTs.

Rab10 dynamic domains are reminiscent of a recently described dynamic ER domain enriched in the ER enzyme Phosphatidylinositol Synthase (PIS)[28]. Photo-activation experiments demonstrated that this dynamic PIS domain is ER-derived [28]. PIS catalyzes the conversion of diacylglycerol precursors and inositol to PI at the ER. To determine if Rab10 and PIS co-localize, we transfected Cos-7 cells with mCh-PIS, BFP-Rab10 and KDEL-venus. We find Rab10 and PIS co-localized at the ER, Golgi, and at dynamic domains (Fig. 5b, Supplementary Movie 2). These dynamic domains are tightly associated with the ER membrane over time, but lack ER luminal marker staining (Fig. 5b, Supplementary Movie 2). Out of 444 puncta (from 10 cells), 68% were positive for both Rab10 and PIS, 24% were Rab10 only positive, and 8% were PIS only positive (Fig. 5c). Thus, Rab10 and PIS co-localize at dynamic ER-associated domains.

Rab10 regulates ER extension and fusion, and partitions with PIS to dynamic ER-associated domains; we therefore asked if these dynamic domains are found at the leading edge of ER extension and fusion events. We acquired live, time-lapse confocal images of Cos-7 cells co-transfected with BFP-Rab10 WT, mCh-PIS, and KDEL-venus (to visualize all ER tubule dynamics) and measured the percent of total dynamics led by a Rab10/PIS punctum (within a 10 μm^2 box over a 5 minute period). This analysis revealed that Rab10/PIS puncta are localized to the leading edge of 42.3% of dynamic events (mean = 4.3 out of 10.2 events, Fig. 5d). Therefore, nearly half, but not all, ER tubule dynamics are led by Rab10/PIS.

To test if the GTP-binding state of Rab10 would affect the ability of Rab10 and PIS to co-localize, we expressed the Rab10 T23N mutant. Rab10 T23N expression reduced the percent of puncta labeled with both markers (to 54%, Fig. 5c). We measured the ability of these Rab10 T23N/PIS puncta to mediate ER extension and fusion and found that the percent of dynamic events led by Rab10/PIS punctum is reduced to 25.9% in the presence of BFP-Rab10 T23N (mean = 1.9 out of 7.3 events, Fig. 5d). Strikingly, when ER dynamic events are led by a Rab10 T23N/PIS punctum, only 11.5%% result in a successful fusion event, compared to 90.7% for Rab10 WT/PIS puncta (Fig. 5e). These data demonstrate that the GTP-binding state of Rab10 regulates the ability of Rab10/PIS dynamic domains to lead and direct ER extension and efficient fusion.

Rab10 regulates the formation of a dynamic domain enriched in PIS and CEPT1

The ER is the major site of synthesis for numerous phospholipids [29]. We therefore asked if other lipid-synthesizing proteins, besides PIS, also localize to Rab10 dynamic domains. At the ER, CEPT1 converts diacylglycerol precursors to phosphatidylethanolamine or phosphatidylcholine [29, 30]. CEPT1 (mCh-tagged) localizes throughout the ER and accumulates at dynamic domains like PIS and Rab10 (Supplementary Fig. 7a–c). Cos-7 cells co-transfected with BFP-Rab10 and mCh-CEPT1 or mCh-PIS show CEPT1 and PIS partitioned to Rab10 dynamic puncta; in contrast, general ER membrane (mCh-Sec61β) or luminal (KDEL-venus) proteins do not (Fig. 6a, b). We quantified this co-localization by using the Pearson-Spearman co-localization coefficient[31], our results show the degree of co-localization is higher between Rab10 and CEPT1 or PIS (69.9% or 70.5%, respectively), than relative to general ER proteins, Sec61β or KDEL (51.3% and 49.8%, respectively, Fig. 6b). We further characterized the composition of dynamic puncta marked by Rab10, PIS,

and/or CEPT1 and found that most puncta are enriched for all three (65.7%) or at least two markers (9.9% for Rab10/CEPT1; 7.7% for Rab10/PIS) (Fig. 7a, Supplementary Fig. 7d, Supplementary Movie 3). Together, these data show that lipid synthesizing proteins partition with Rab10 to dynamic domains, and introduce the possibility that phospholipid synthesis is coupled to Rab10-mediated ER extension and fusion.

We next asked if co-localization of PIS and CEPT1 to dynamic puncta requires functional Rab10. Expression of GDP-locked mutant Rab10 T23N results in a dramatic decrease in the accumulation of CEPT1 at dynamic puncta, as well as a reduction in the size of PIS-labeled puncta (Fig. 7b, Supplementary Movie 4). We also tested the effect of Rab10 T23N expression on PIS puncta dynamics by overlaying time-lapse snapshots of GFP-PIS taken at t_0 and t_{60sec}, and measuring the extent of PIS punctum movement over time (Fig. 7c). Using the Pearson-Spearman co-localization coefficient to quantitate these data, we found that PIS puncta are less mobile in the presence of Rab10 T23N compared to Rab10 WT (33.7% versus 56.2%, respectively, Fig. 7d). Together, these data demonstrate the requirement of functional Rab10 for the formation and dynamics of the Rab10/PIS/CEPT1 domain.

Atlastin and Rab10 do not overlap in function or location

Rab10 dynamic domains do not lead all ER dynamics; however, the atlastin fusion machinery[5–7] could be responsible for the remaining events. Atlastin is ubiquitously expressed, partitions specifically to ER tubules and accumulates at 3-way junctions[5–7, 32, 33]. We localized GFP-Atl3 to ER tubules and to punctate structures at 3-way junctions (Fig. 8a). These GFP-Atl3 puncta do not co-localize with the Rab10 dynamic puncta (Fig. 8b). Expression of GFP-Atl3 is unable to rescue the expansion of ER cisternae caused by BFP-Rab10 T23N expression or Rab10 siRNA treatment (Fig. 8b, c). In fact, lack of functional Rab10 alters the localization of GFP-Atl3. Atlastin puncta also do not co-localize with dynamic domains labeled by Rab10 and PIS (Fig. 8d, Supplementary Movie 5). Indeed, depletion of Atlastin or Rab10 give nearly opposite ER phenotypes: atlastin depletion from Cos-7 cells results in elongated ER tubules[5], while Rab10 depletion leads to a reduction in tubular ER (Fig. 3). Thus, Rab10 and atlastin machineries likely regulate separate and non-redundant aspects of ER dynamics (see model in Supplementary Fig. 8a).

DISCUSSION

We have demonstrated that Rab10 localizes to the ER and regulates ER tubule dynamics. Rab10 depletion or expression of a GDP-locked Rab10 mutant reduces both the frequency of ER tubule extension and the efficiency of ER tubule fusion (see model in Supplementary Fig. 8b). Consequently, the absence of functional Rab10 leads to a more cisternal and less tubular ER morphology; a phenotype similar to depletion of reticulon proteins[16, 26] or depolymerization of MTs[2]. Rab10 has a unique localization complementing its function by accumulating in a dynamic domain positioned at the leading edge of nearly half of all ER tubule dynamics. These Rab10 dynamic domains do not initially label with ER luminal or membrane proteins, but predict the path of where the growing ER tubule will travel.

A particularly compelling feature of the studied Rab10 dynamic domains is that these domains also accumulate at least two proteins involved in phospholipid biogenesis (see

model in Supplementary Fig. 8a). These proteins, CEPT1 and PIS, are each integral membrane proteins of the ER, yet, they partition with Rab10 at the leading edge of ER dynamics. Even though the Rab10 dynamic domain does not label with luminal or general ER membrane proteins, the localization of the ER proteins PIS and CEPT1 at this domain suggest that it is continuous with the ER membrane. Previous data demonstrate that dynamic domains containing PIS are either continuous with or derived from the ER[28]. Kim, et al. showed photoactivatable GFP-tagged PIS when activated eventually localizes to structures at the dynamic ends of the ER[28]. Here we show that functional Rab10 is required for CEPT1 and PIS to co-localize and partition to dynamic domains within the ER. Our studies have not yet addressed if CEPT1 and PIS are similarly required for Rab10 dynamic domain formation.

A popular theory posits that Rabs and components of the phospholipid synthesis pathway confer not only membrane identity, but also recruit other necessary components to regulate different parts of the fusion process[8, 9, 34]. Based on the co-localization between Rab10, PIS and CEPT1 at the leading edge of dynamic ER events and the requirement of functional Rab10 for the formation of this dynamic domain, we suggest that a Rab10 complex could mediate ER extension and fusion along the MT cytoskeleton, while PIS and CEPT1 could synthesize the phospholipids necessary for ER growth and/or fusion (Supplementary Fig. 8). Together, these connections introduce the intriguing model that new ER tubule growth, fusion and phospholipid synthesis could all be coupled. It remains to be determined if active lipid synthesis occurs in Rab10/PIS/CEPT1 structures located at the leading edge of ER tubule dynamics and if so, what effect blocking phospholipid synthesis at these positions would have on ER tubule dynamics. An alternative possibility is that lipid synthesis does not drive ER tubule growth, but rather the synthesis of specific phospholipids at the tip of dynamic ER tubules facilitates transfer of these phospholipids to other membrane bound compartments during ER dynamics. This theory was initially proposed by Kim, et al. in their description of PIS dynamic domains[28]. However, the PIS dynamic domains did not co-localize with any of the organelle markers tested[28], but it is possible that transfer could occur during transient contacts. Future studies will be required to determine if there is a physical link between Rab10 and these lipid-synthesizing enzymes or with molecular motor proteins.

ONLINE METHODS

In vitro ER formation and Aequorin-Based Ca^{2+} Efflux Assay

A light membrane fraction from *Xenopus* egg extracts was prepared as previously described [15]. ER formation assays were performed by washing membranes one time in membrane wash buffer (MWB = 50 mM HEPES-KOH [pH 7.5], 2.5 mM $MgCl_2$, 250 mM sucrose, 150 mM KCl), followed by incubation in MWB with 1 mM ATP and 0.5 mM GTP at 25°C for 60 min according to methods described [16]. Network staining was performed with octadecyl rhodamine and *in vitro* networks were visualized by fluorescence microscopy. Aequorin luminescence assays were preformed as previously described [16], with measurements taken every 2.5 min.

GTP-binding Protein Precipitation and Mass Spectrometry

A light membrane fraction from *Xenopus* eggs was prepared as previously described [15]. Membranes were incubated for 5 min at room temperature in high salt MWB (MWB with 500 mM KCl). The high salt washed membranes were then solubilized in 1% digitonin and centrifuged, the pelleted fraction was discarded. GTPγS samples were incubated with 1 mM GTPγS for 10 min at room temperature. Both sets of solubilized membranes were bound to GTP-agarose beads in 150 mM MWB for 1 hr at room temperature. Bound proteins were eluted with 10 mM GTP, subjected to SDS-PAGE and identified by mass spectrometry. All mass spectrometry was performed by the Taplin MS facility at Harvard Medical School.

Constructs

KDEL-venus was a gift from E. Snapp (Albert Einstein College of Medicine). GPP130-eGFP was a gift from T. Lee (Carnegie Mellon University). mCh-KDEL, GFP-mito, GFP-Rab7 and mCh-α-Tubulin were gifts from J. Friedman. mCh-Sec61β was described previously[35]. mCh-Rab5 was described previously [27]. GFP-Atl3 was a gift from Jonathan Friedman and generated by PCR amplifying full length Atl3 (NCBI NM_015459) and cloning into the KpnI/XhoI sites of the pAcGFP-C1 vector (Clonetech). mCh-Climp63 was a gift from Jonathan Friedman and generated by PCR amplifying full length Climp63 (NCBI NM_006825) and cloning into the NheI/BamHI from mCh-α-Tubulin. GFP-PIS was generated by PCR amplifying full length PIS (NCBI AF014807) and cloning into the BglII/KpnI sites of the pAcGFP-C1 vector. mCh-PIS was generated by PCR amplifying full length PIS (NCBI AF014807) and cloning into the BglII/KpnI sites of pAcGFP-C1, pAcGFP-C1 had GFP excised and mCherry inserted into NheI/XhoI sites. mCh-CEPT1 was generated by PCR amplifying full length CEPT1 (NCBI NM_006090) and cloning into the BglII/EcoRI sited of pAcGFP-C1, pAcGFP-C1 had GFP excised and mCherry inserted into NheI/XhoI sites. mCh-Rab8, mCh-Rab10 and mCh-Rab11 were generated by cloning mCherry into the NheI/BglII sites of pAcGFP1-N1 (Takara Bio Inc.) and cloning human Rab8 (NCBI NM_016530), human Rab10 (NCBI NM_016131) or human Rab11 (NCBI NM_004663) with a stop codon into the BglII/EcoRI sites of that vector. mCh-Rab10 Q68L and T23N were generated by site directed mutagenesis from mCh-Rab10. BFP-Rab10 was generated by PCR amplifying full length Rab10 and cloning into the BglII/EcoRI sites of pTagBFP-C. BFP-Rab10 T23N was generated by site directed mutagenesis from BFP-Rab10. mCh-Rab5 S34N was generated by site directed mutagenesis from mCh-Rab5.

Expression in Mammalian Tissue Culture Cells

Cos-7 and HeLa cells (ATCC) were grown to 80% confluency in Dulbecco's Modified Eagle Medium High Glucose (12430-062, Invitrogen) with 10% FBS and 1% penicillin/streptomycin in 3.5 cm microscope dish (P35G-2-14-CGRD, MatTek). Plasmid transfections were performed in Opti-MEM media (31985-088, Invitrogen) with 5 μL Lipofectamine 2000 (11668-027, Invitrogen) per dish for 5 hours. Cells were imaged 36–48 hours after transfection was completed. For all experiments, the following amounts of DNA were transfected per well: 0.25 μg mCh-Rab5; 0.25 μg mCh-Rab5 S34N; 0.25 μg GFP-Rab7; 0.25 μg mCh-Rab8; 0.5 μg mCh-Rab10; 0.5 μg mCh-Rab10 Q68L; 0.5 μg mCh-Rab10 T23N; 0.5 μg BFP-Rab10; 0.5 μg BFP-Rab10 T23N; 0.25 μg mCh-Rab11; 0.1 μg

KDEL-venus; 0.25 μg mCh-KDEL; 0.5 μg mCh-Sec61β; 50 ng GFP-mito; 50 ng GPP130-GFP; 0.25 μg mCh-Climp63; 0.125 μg mCh-α-tubulin; 0.2 μg GFP-PIS; 0.2 μg mCh-PIS; 0.2 μg mCh-CEPT1; 0.1 μg GFP-Atl3.

siRNA Transfections

Cos-7 cells were grown to 80% confluency in Dulbecco's Modified Eagle Medium High Glucose with 10% FBS in 6 cm tissue culture dishes. Transfections were performed, following manufactures directions, using DharmaFECT #1 transfection reagent (T-2001-02, Dharmacon). In brief, Negative Control (AM4635, Applied Bioscience) or Rab10 SMARTpool siRNA (L-010823-00-0005, Dharmacon, target sequences: GCAAGGGAGCAUGGUAUUA, CACGUUAGCUGAAGAUAUC, GAUGAUGCCUUCCAAUACUA, and GAAUAGACUUCAAGAUCAA) were mixed with the transfection reagent to a final concentration of 25 nM, then applied to the cells for 48 hours. In addition, various fluorescent plasmids were transfected, following manufactures directions, into each dish using Lipofectamine 2000 transfection reagent. The transfection was terminated by removing the transfection media and splitting the cells to a 3.5 cm microscope dish and a 6 cm tissue culture dish. After 24 hours the cells in the 3.5 cm microscope dish were imaged and the cells in the 6 cm tissue culture dish were harvested for protein level analysis by western blot.

Immuno-blot Analysis and Densitometry

Whole cell lysates of Cos-7 cells were resuspended in Laemmli sample buffer, boiled 10 min, separated by SDS-PAGE, and transferred to PVDF membrane. Primary antibodies to Rab10 (1:500, #8127S, Cell Signaling Technologies) and GAPDH (1:30,000, #G9545, Sigma), and HRP-conjugated goat anti-rabbit (1:3,000, #A6154, Sigma) secondary antibodies were used. Signal was detected with SuperSignal West Pico Chemiluminescent solution (34080, Thermo Fisher Scientific). Relative protein levels were determined using the ImageJ (NIH) Gel Plotting Macro following the protocol outlined in the ImageJ instruction manual.

Confocal Microscopy

Confocal Z-stacks of the peripheral ER were collected using Metamorph Software (Molecular Devices) on a Nikon Eclipse TE2000-U with a 100x objective, 1.40 NA (Nikon), fitted with a spinning disk confocal system (Solamere Technology Group,) and a Cascade II, a 16 bit EMCCD camera with a chip size 512 × 512 pixels (Photometrics) (pixel size at 1000x = 0.09 μm/pixel) (step size = 0.25μm). Excitation of the fluorophores was performed using 405, 473 and 561nm diode LASERs.

ER Cisternae Analysis

The Z-stacks were imported to ImageJ (NIH) for analysis. Each Z-stack was first compressed to a Maximum Intensity Projection. The displayed range of the projection was set to the minimum and maxim intensities of the image. The image was then converted from a bit depth of 16 to 8, where the minimum intensity of the 16 bit image was 0 in the 8 bit image, and the maximum intensity of the 16 bit image was 255. Using the Reni Entropy

Threshold setting, the 8 bit projection image was then converted to two separate binary thresholded images [36]. The first image represents ER cisternae and the second image represents total ER. Three identical 28 pixel wide line segments were drawn on the thresholded images, beginning at the nuclear envelope and ending at the cell periphery (while avoiding the MT organizing center). To determine the area in pixels of ER covered by each line segment, we first measured the total area in pixels and the mean intensity of each line segment, then divided the product of the mean intensity and the area by 255. Dividing the number of ER cisternae pixels by the number of total ER pixels gives the percentage of ER cisternae in each line segment. The remaining ER was determined to be ER tubes.

ER Dynamics Analysis

After imaging for 5 min, with exposures every 10 sec, the timecourses were imported to ImageJ (NIH) for analysis. Brightness and contrast was adjusted across the images using ImageJ. The timecourses were analyzed frame by frame for fusion events and for the presence of Rab10/PIS punctum, when applicable. Where indicated, nocodazole (Acros Organics) drug treatments were preformed as previously described [27].

Pearson-Spearman co-localization coefficient

Acquired Z-stacks or one minute timecourses were imported to ImageJ (NIH) for analysis. Each Z-stack was first compressed to a Maximum Intensity Projection. The displayed range of the projection was set to the minimum and maxim intensities of the image. The image was then converted from a bit depth of 16 to 8, where the minimum intensity of the 16 bit image was 0 in the 8 bit image, and the maximum intensity of the 16 bit image was 255. The necessary images were overlayed and the Pearson-Spearman co-localization coefficient was determined using the PSC Colocalization plugin[31] for ImageJ.

Statistical Analysis

Statistical significance between two values was determined using a two tailed, unpaired Student's *t* test (Graphpad Prism). Statistical analysis of three or more values was performed by one way ANOVA with Tukey's post hoc test (Graphpad Prism). All data are presented as the mean ± standard error of the mean; *** $P < 0.001$, ** $P < 0.01$.

Supplementary Material

Refer to Web version on PubMed Central for supplementary material.

Acknowledgments

We thank C. English for helpful suggestions, A. Merz for generously providing Rab GDI, and E. Snapp, T. Lee, and J. Friedman for constructs. This work was supported by NIH grants GM083977 to GKV and GM07135 to ARE.

References

1. Lee C, Chen LB. Dynamic behavior of endoplasmic reticulum in living cells. Cell. 1988; 54:37–46. [PubMed: 3383243]

2. Terasaki M, Chen LB, Fujiwara K. Microtubules and the endoplasmic reticulum are highly interdependent structures. J Cell Biol. 1986; 103:1557–1568. [PubMed: 3533956]
3. Waterman-Storer CM, Salmon ED. Endoplasmic reticulum membrane tubules are distributed by microtubules in living cellsusing three distinct mechanisms. Curr Biol. 1998; 8:798–806. [PubMed: 9663388]
4. English AR, Zurek N, Voeltz GK. Peripheral ER structure and function. Curr Opin Cell Biol. 2009; 21:596–602. [PubMed: 19447593]
5. Hu J, et al. A class of dynamin-like GTPases involved in the generation of the tubular ER network. Cell. 2009; 138:549–561. [PubMed: 19665976]
6. Orso G, et al. Homotypic fusion of ER membranes requires the dynamin-like GTPase atlastin. Nature. 2009; 460:978–983. [PubMed: 19633650]
7. Rismanchi N, Soderblom C, Stadler J, Zhu PP, Blackstone C. Atlastin GTPases are required for Golgi apparatus and ER morphogenesis. Hum Mol Genet. 2008; 17:1591–1604. [PubMed: 18270207]
8. Murray JT, Panaretou C, Stenmark H, Miaczynska M, Backer JM. Role of Rab5 in the recruitment of hVps34/p150 to the early endosome. Traffic. 2002; 3:416–427. [PubMed: 12010460]
9. Behnia R, Munro S. Organelle identity and the signposts for membrane traffic. Nature. 2005; 438:597–604. [PubMed: 16319879]
10. Pfeffer SR. Rab GTPases: specifying and deciphering organelle identity and function. Trends Cell Biol. 2001; 11:487–491. [PubMed: 11719054]
11. Cai H, Reinisch K, Ferro-Novick S. Coats, tethers, Rabs, and SNAREs work together to mediate the intracellular destination of a transport vesicle. Dev Cell. 2007; 12:671–682. [PubMed: 17488620]
12. Schwartz SL, Cao C, Pylypenko O, Rak A, Wandinger-Ness A. Rab GTPases at a glance. J Cell Sci. 2007; 120:3905–3910. [PubMed: 17989088]
13. Turner MD, Plutner H, Balch WE. A Rab GTPase is required for homotypic assembly of the endoplasmic reticulum. J Biol Chem. 1997; 272:13479–13483. [PubMed: 9153191]
14. Audhya A, Desai A, Oegema K. A role for Rab5 in structuring the endoplasmic reticulum. J Cell Biol. 2007; 178:43–56. [PubMed: 17591921]
15. Dreier L, Rapoport TA. In vitro formation of the endoplasmic reticulum occurs independently of microtubules by a controlled fusion reaction. J Cell Biol. 2000; 148:883–898. [PubMed: 10704440]
16. Voeltz GK, Prinz WA, Shibata Y, Rist JM, Rapoport TA. A class of membrane proteins shaping the tubular endoplasmic reticulum. Cell. 2006; 124:573–586. [PubMed: 16469703]
17. Bucci C, Thomsen P, Nicoziani P, McCarthy J, van Deurs B. Rab7: a key to lysosome biogenesis. Mol Biol Cell. 2000; 11:467–480. [PubMed: 10679007]
18. Bucci C, et al. Co-operative regulation of endocytosis by three Rab5 isoforms. FEBS Lett. 1995; 366:65–71. [PubMed: 7789520]
19. Ullrich O, Reinsch S, Urbe S, Zerial M, Parton RG. Rab11 regulates recycling through the pericentriolar recycling endosome. J Cell Biol. 1996; 135:913–924. [PubMed: 8922376]
20. Chen W, Wandinger-Ness A. Expression and functional analyses of Rab8 and Rab11a in exocytic transport from trans-Golgi network. MethodsEnzymol. 2001; 329:165–175.
21. Schuck S, et al. Rab10 is involved in basolateral transport in polarized Madin-Darby canine kidney cells. Traffic. 2007; 8:47–60. [PubMed: 17132146]
22. Shi A, et al. EHBP-1 functions with RAB-10 during endocytic recycling in Caenorhabditis elegans. Mol Biol Cell. 2010; 21:2930–2943. [PubMed: 20573983]
23. Chen CC, et al. RAB-10 is required for endocytic recycling in the Caenorhabditis elegans intestine. Mol Biol Cell. 2006; 17:1286–1297. [PubMed: 16394106]
24. Stenmark H, et al. Inhibition of rab5 GTPase activity stimulates membrane fusion in endocytosis. EMBO J. 1994; 13:1287–1296. [PubMed: 8137813]
25. Shibata Y, et al. Mechanisms determining the morphology of the peripheral ER. Cell. 2010; 143:774–788. [PubMed: 21111237]

26. Anderson DJ, Hetzer MW. Reshaping of the endoplasmic reticulum limits the rate for nuclear envelope formation. J Cell Biol. 2008; 182:911–924. [PubMed: 18779370]
27. Friedman JR, Webster BM, Mastronarde DN, Verhey KJ, Voeltz GK. ER sliding dynamics and ER-mitochondrial contacts occur on acetylated microtubules. J Cell Biol. 2010; 190:363–375. [PubMed: 20696706]
28. Kim YJ, Guzman-Hernandez ML, Balla T. A highly dynamic ER-derived phosphatidylinositol-synthesizing organelle supplies phosphoinositides to cellular membranes. Dev Cell. 2011; 21:813–824. [PubMed: 22075145]
29. Fagone P, Jackowski S. Membrane phospholipid synthesis and endoplasmic reticulum function. J Lipid Res. 2009; 50 (Suppl):S311–316. [PubMed: 18952570]
30. Henneberry AL, Wright MM, McMaster CR. The major sites of cellular phospholipid synthesis and molecular determinants of Fatty Acid and lipid head group specificity. Mol Biol Cell. 2002; 13:3148–3161. [PubMed: 12221122]
31. French AP, Mills S, Swarup R, Bennett MJ, Pridmore TP. Colocalization of fluorescent markers in confocal microscope images of plant cells. Nat Protoc. 2008; 3:619–628. [PubMed: 18388944]
32. Park SH, Zhu PP, Parker RL, Blackstone C. Hereditary spastic paraplegia proteins REEP1, spastin, and atlastin-1 coordinate microtubule interactions with the tubular ER network. J Clin Invest. 2010; 120:1097–1110. [PubMed: 20200447]
33. Chen S, Novick P, Ferro-Novick S. ER network formation requires a balance of the dynamin-like GTPase Sey1p and the Lunapark family member Lnp1p. Nat Cell Biol. 2012
34. Wenk MR, De Camilli P. Protein-lipid interactions and phosphoinositide metabolism in membrane traffic: insights from vesicle recycling in nerve terminals. Proc Natl Acad Sci U S A. 2004; 101:8262–8269. [PubMed: 15146067]
35. Zurek N, Sparks L, Voeltz G. Reticulon short hairpin transmembrane domains are used to shape ER tubules. Traffic. 2011; 12:28–41. [PubMed: 20955502]
36. Sahooa PK, Arorab G. A thresholding method based on two-dimensional Renyi's entropy. Pattern Recognition. 2004; 37:1149–1161.

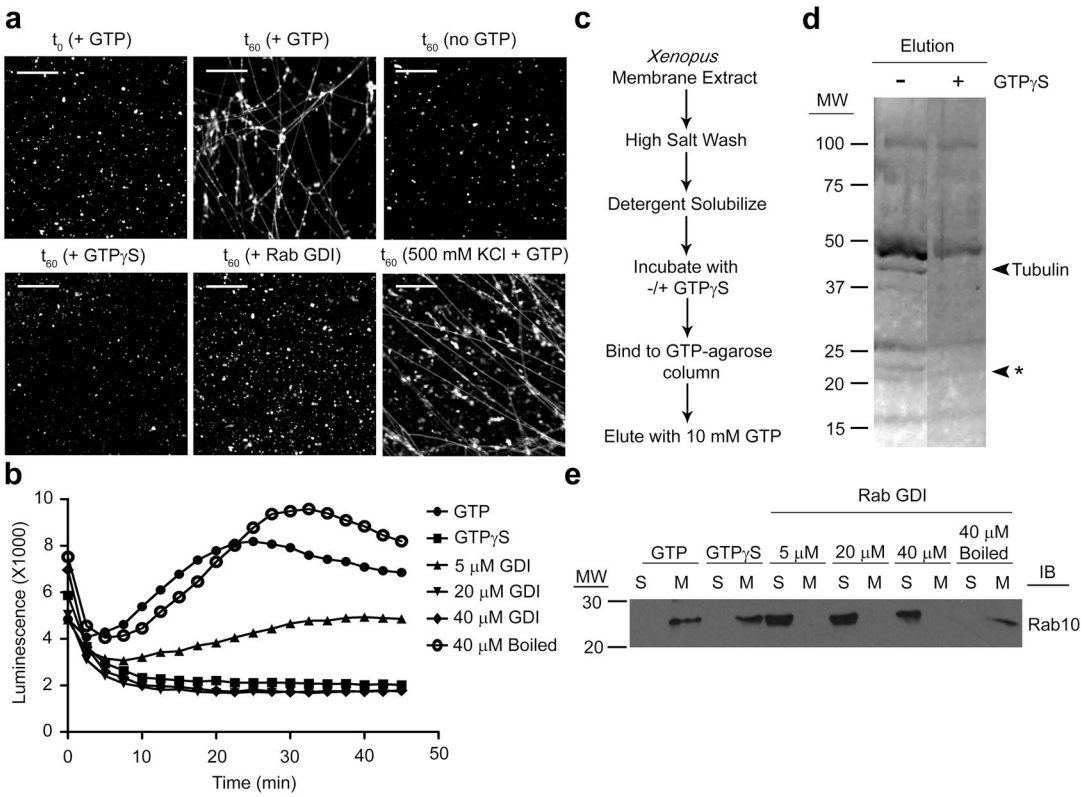

Figure 1. Purification of GTP binding proteins from a *Xenopus laevis in vitro* ER assembly assay

a, ER vesicles from fractionated *Xenopus laevis* eggs were analyzed directly (t_0) or incubated for 60 min (t_{60}) at 25°C with GTP, no GTP, GTPγS. Alternatively, vesicles were pre-incubated for 20 min at 25°C with Rab GDI or washed with 0.5 M KCl buffer and then incubated with GTP. The resulting vesicles or tubules were visualized by fluorescence microscopy with octadecyl rhodamine. Scale bars = 10 μm. **b,** Ca^{2+} efflux from ER vesicles was measured with aequorin in a luminometer during the course of an ER tubule formation assay. The reactions were performed in the presence of GTP, GTP + GTPγS, or GTP following preincubation with 5 μM Rab GDI, 20 μM Rab GDI, 40 μM Rab GDI, or 40 μM boiled Rab GDI. **c,** Strategy used to purify GTP-binding proteins from ER vesicles. **d,** Bound proteins from purification shown in **c** were eluted with GTP and analyzed by SDS-PAGE and silver staining. Control samples were pre-incubated with GTPγS before application to GTP-agarose column (second lane). Arrowheads mark bands analyzed by mass spectrometry. Asterisk indicates the isolated band that identified Rab11, Rab8/10, Rab7, Rab2, and Rab1. **e,** Reactions in **b** were alternatively spun down and separated into soluble (S) and membrane (M) fractions. Soluble and membrane proteins were analyzed by immuno-blotting (IB) with antibodies recognizing *Xenopus* Rab8/10. Note that Rab 8/10 is displaced from the ER vesicles by concentrations of Rab GDI that inhibit tubule formation (as assayed in **a** and **b**).

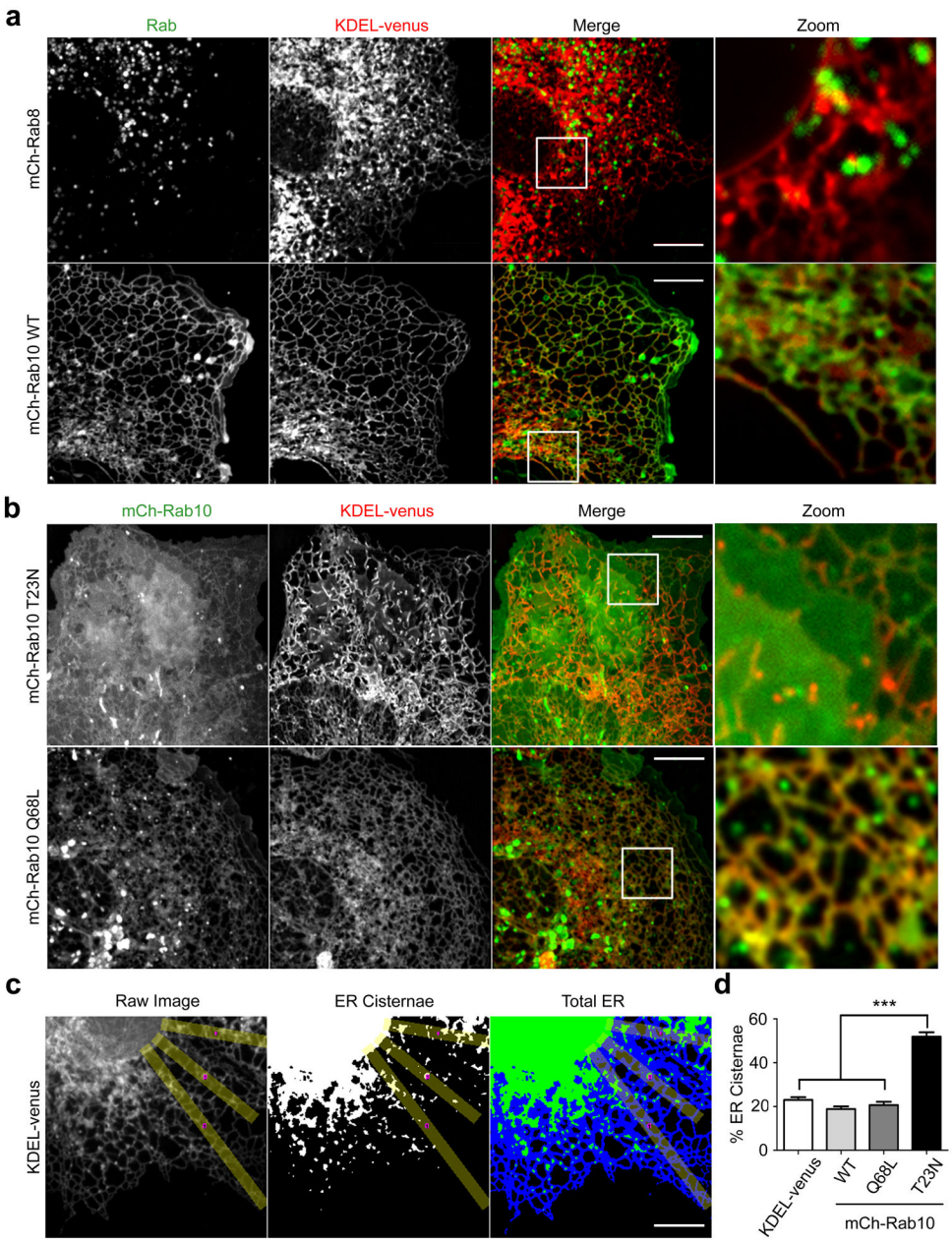

Figure 2. Rab10 localizes to the ER and regulates tubular ER morphology

a, Cos-7 cells co-expressing mCh-tagged human Rab8 (mCh-Rab8) or Rab10 (mCh-Rab10) and a luminal ER protein (KDEL-venus) were localized by confocal FM (top and bottom panels, respectively). Third and fourth panels show merged image and zoom of boxed region, respectively (Rab in green, ER in red). Note that Rab10 localizes throughout the ER, and Rab8 does not. **b,** As in **a** for cells expressing KDEL-venus with mCh-Rab10 T23N or mCh-Rab10 Q68L, as indicated. Note the expansive cisternae in Rab10 T23N expressing cells. **c,** Method for quantitative analysis of ER shape. Three identical 28 pixel wide line segments were drawn on the images beginning at the NE away from the MT organizing center (yellow boxes), the Reni Entropy Threshold setting was used to select only ER

cisternae (middle panel image) or the total ER (third panel, green + blue). Dividing the number of ER cisternae pixels (green) by the number of total ER pixels (green + blue) gives the percentage of ER cisternae in each line segment. The remaining ER was defined as ER tubules. For **a**, **b** and **c**, scale bars = 10 μm. **d,** Percentage of the ER comprised of cisternae (using analysis described in **c**) for cells expressing KDEL-venus alone or together with mCh-Rab10 WT, mCh-Rab10 Q68L, or mCh-Rab10 T23N. Means ± standard errors were calculated from each condition in **d**, n = 50 cells for each condition, 3 regions per cell. *** $P < 0.001$..

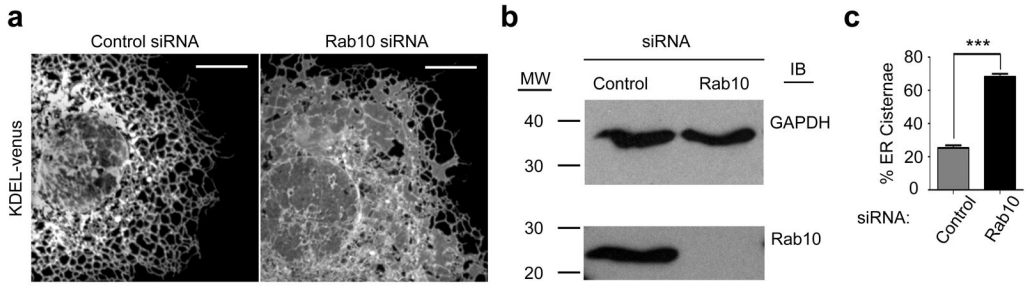

Figure 3. Depletion of endogenous Rab10 reduces tubular ER morphology

a, Cos-7 cells were co-transfected with a luminal ER marker (KDEL-venus) and either control or Rab10 siRNA, and were then visualized by confocal FM to detect changes in ER morphology (note the expansive cisternae in the Rab10 siRNA depleted sample). Scale bars = 10 μm. **b,** Immuno-blot analysis with antibodies against Rab10 reveals efficient depletion of Rab10 by siRNA. GAPDH protein levels were measured as a loading control. **c,** Percentage of the ER comprised of cisternae for cells transfected as in **a** with control or Rab10 siRNA (analysis performed as described in Fig. 2c and 2d). Means ± standard errors were calculated from each condition, n = 50 cells, 3 regions per cell. *** $P < 0.001$.

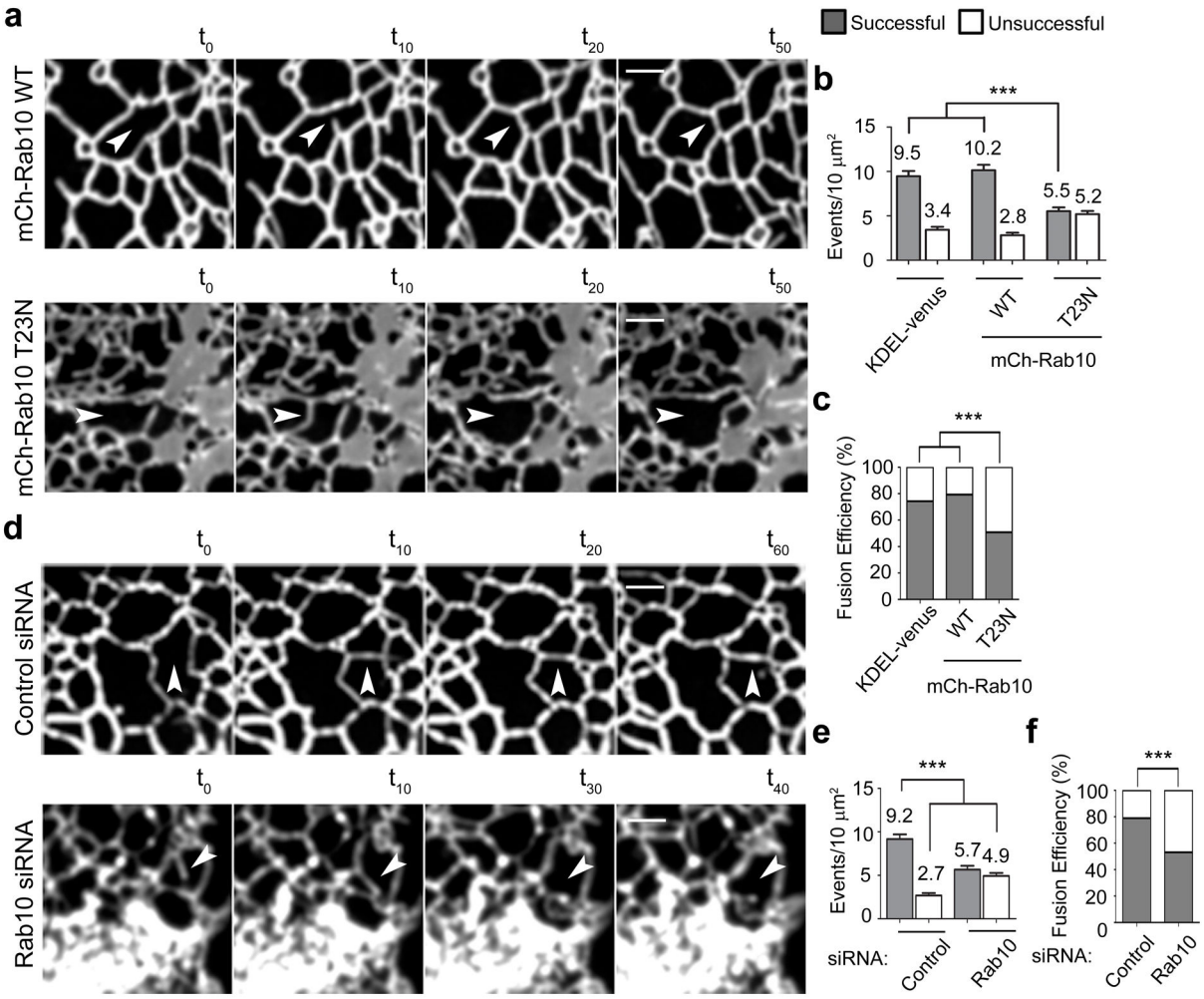

Figure 4. Rab10 regulates ER tubule dynamics and fusion

a, Cos-7 cells expressing KDEL-venus and mCh-Rab10 WT or mCh-Rab10 T23N (top and bottom panel, respectively) were imaged live to visualize ER tubule extension and fusion events at time points indicated (in seconds). Arrowheads mark the sites of successful (top panels) or unsuccessful fusion (bottom panels). **b,** Cells described in **a** were imaged live to measure the number of tubular ER extension events that occurred in a 10 μm^2 box over a 5 min time course. These tubular extensions were scored as either resulting in a successful or unsuccessful fusion event. **c,** The successful and unsuccessful fusion events measured in **b** were alternatively graphed as a percentage of events leading to fusion. **d,** Cos-7 cells expressing KDEL-venus to visualize ER extension and fusion were co-transfected with control siRNA (top panel) or Rab10 siRNA (bottom panel) and were imaged at the indicated time points (in seconds). Arrowheads mark sites of successful fusion (top panel) or unsuccessful fusion (bottom panel). Images in **a** and **d,** scale bars = 2 μm.. **e,** As in **b** for **d. f,** As in **c** for **d**. Means ± standard errors were calculated for **b**, **c**, **e** and **f**, n = 30 cells for each condition, 2 boxes for each cell. *** P < 0.001.

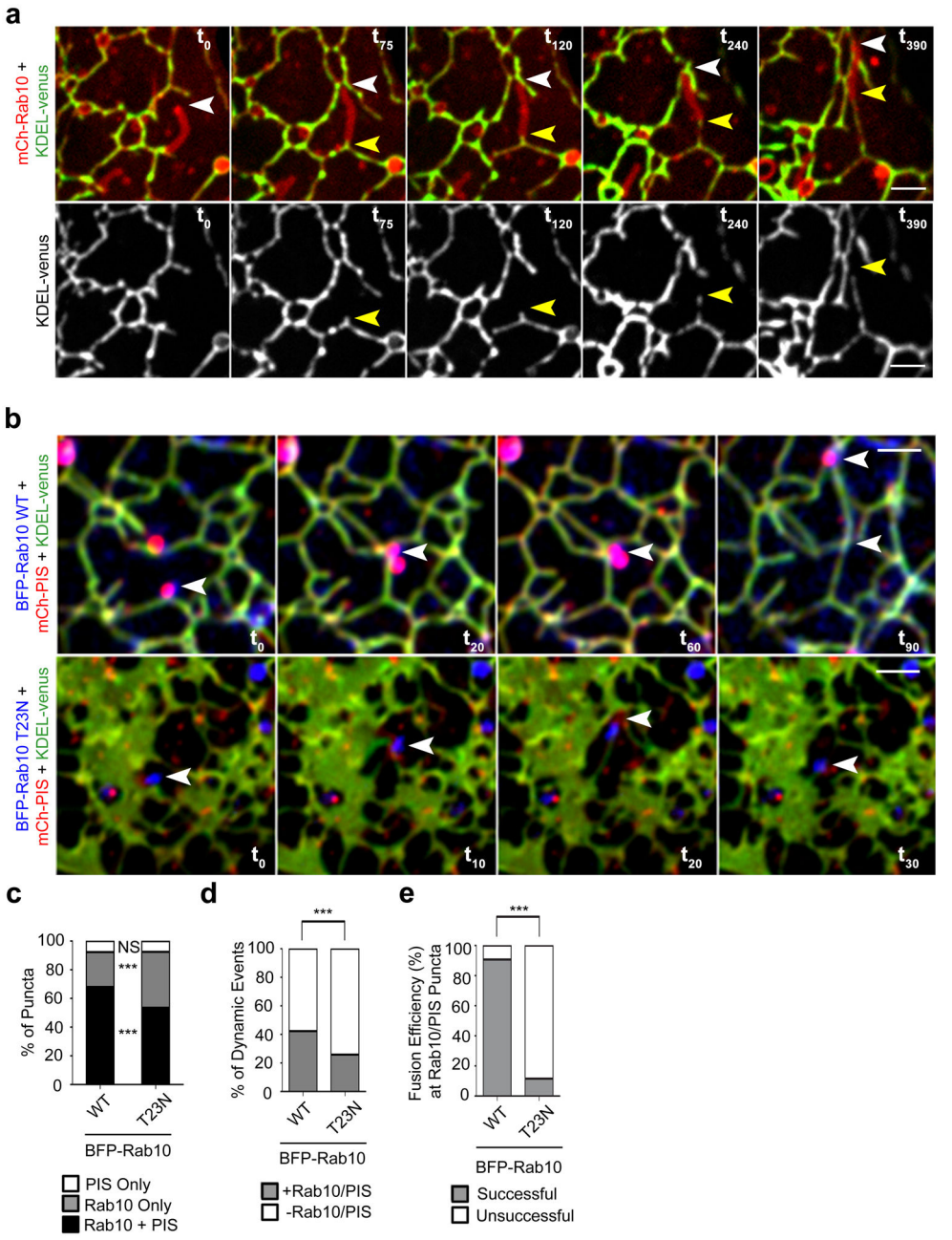

Figure 5. Rab10 and PIS co-localize to the leading edge of ER dynamics

a, A Cos-7 cell co-expressing luminal ER marker (KDEL-venus) and mCh-Rab10 imaged by live confocal FM to visualize ER dynamics; top panel shows overlay, bottom panel shows KDEL-venus alone to illustrate the absence of the ER from the Rab10 domain. Arrowheads mark the position of a Rab10 dynamic domain (in red, white arrowhead) not initially labeled with the luminal ER marker (in green, yellow arrowhead follows movement of KDEL marker behind the Rab10 domain). **b,** As in **a** for cells expressing KDEL-venus, mCh-tagged human PIS (mCh-PIS) and either BFP-Rab10 WT (top panel) or BFP-Rab10 T23N (bottom panel) (PIS in red, Rab10 in blue, KDEL in green). Note that Rab10 and PIS

co-localize at dynamic domains not initially labeled with KDEL. Arrowheads mark positions of successful and unsuccessful fusion events (top and bottom panel, respectively) that follow the BFP-Rab10/mCh-PIS dynamic domain structures. Images in **a** and **b**, scale bars = 2 μm.. **c,** Percentage of ER attached puncta that contain both BFP-Rab10 and mCh-PIS, BFP-Rab10 alone, or mCh-PIS alone (n = 444 puncta for BFP-Rab10 WT and 492 puncta for BFP-Rab10 T23N). **d,** Cos-7 cells co-transfected as in **b** and imaged live by confocal FM. All ER extension events occurring in a 10 μm^2 box over a 5 min time course were observed. We calculated the percentage of total events clearly led by either a PIS/Rab10 WT or PIS/Rab10 T23N dynamic domain (621 and 437 total events, respectively). **e,** For each of the events in **d** led by a PIS/Rab10 dynamic domain, we scored if the event led to a successful fusion reaction with adjacent ER domains. The efficiency of fusion was calculated for puncta containing WT or T23N Rab10. Note that PIS/Rab10 T23N puncta had a highly reduced ability to successfully fuse. All times indicated are in seconds. Means ± standard errors were calculated for each graph; for **c,** n = 10 cells; for **d** and **e,** n = 30 cells, 2 boxes per cell. *** $P < 0.001$.

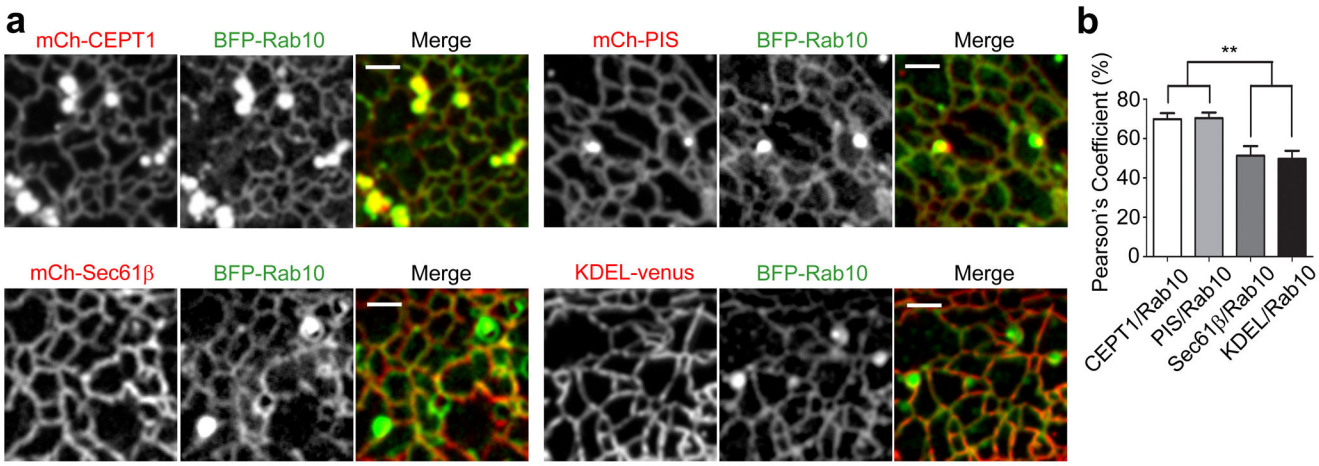

Figure 6. CEPT1 and PIS partition with Rab10 to ER-associated dynamic domains

a, A Cos-7 cell expressing BFP-Rab10 with mCh-CEPT1 (first panel), mCh-PIS (second panel), mCh-Sec61β (third panel) or KDEL-venus (fourth panel). Left image shows mCh-CEPT1, mCh-PIS, mCh-Sec61β or KDEL-venus, respective of panel; middle image shows BFP-Rab10. Right image shows merge for each condition. Scale bars = 2 μm.. **b,** Percentage of co-localization for cells expressing BFP-Rab10 with mCh-CEPT1, mCh-PIS, mCh-Sec61β or KDEL-venus, as measured by Spearman-Pearson's co-localization coefficient in a 10 μm^2 box. Note that CEPT1 and PIS are enriched in a domain with Rab10 relative to the other ER markers tested. Means ± standard errors were calculated from each condition, n = 10 cells for each condition. ** $P < 0.01$.

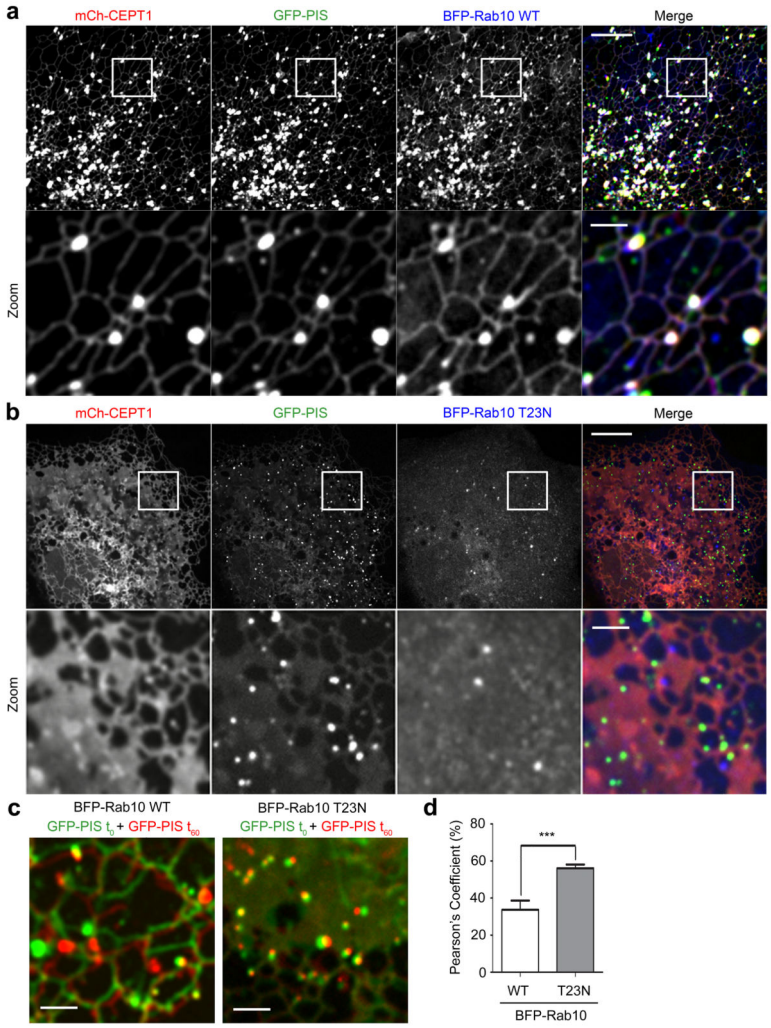

Figure 7. Rab10 regulates the formation of Rab10/PIS/CEPT1 dynamic puncta

a, A Cos-7 cell co-expressing mCh-CEPT, GFP-PIS and BFP-Rab10 WT (CEPT1 in red, PIS in green, Rab10 WT in blue). Note that CEPT1, PIS and Rab10 co-localize throughout the ER and at punctate structures. **b,** A Cos-7 cell co-expressing mCh-CEPT, GFP-PIS and BFP-Rab10 T23N (CEPT1 in red, PIS in green, Rab10 T23N in blue). Note that CEPT1 no longer forms punctate structures and PIS puncta are markedly smaller. For **a** and **b**, third and fourth panels show merged image and zoom of boxed region, respectively, top panel scale bars = 10 μm, bottom panel scale bars = 2 μm.. **c,** Cells as in **a** and **b** were imaged live, with two images acquired, taken 1 minute apart. These images were superimposed in order to visualize the change in GFP-PIS over a 1 minute time period with BFP-Rab10 WT (left panel) or BFP-Rab10 T23N (right panel) expression. Each image shows GFP-PIS at t = 0 (green) and t = 60 s (red). Immobile puncta will appear yellow. Note that the 60 second overlay for GFP-PIS expressed with BFP-Rab10 T23N shows very little change in PIS dynamics. Scale bars = 2 μm. **d,** Percentage of co-localization for cells expressing GFP-PIS withBFP-Rab10 WT or BFP-Rab10 T23N, as measured by Spearman-Pearson's co-localization coefficient. Note that the higher the percentage co-localization, the less overall

dynamics. Means ± standard errors were calculated from each condition, n = 10 cells for each condition. *** P < 0.001.

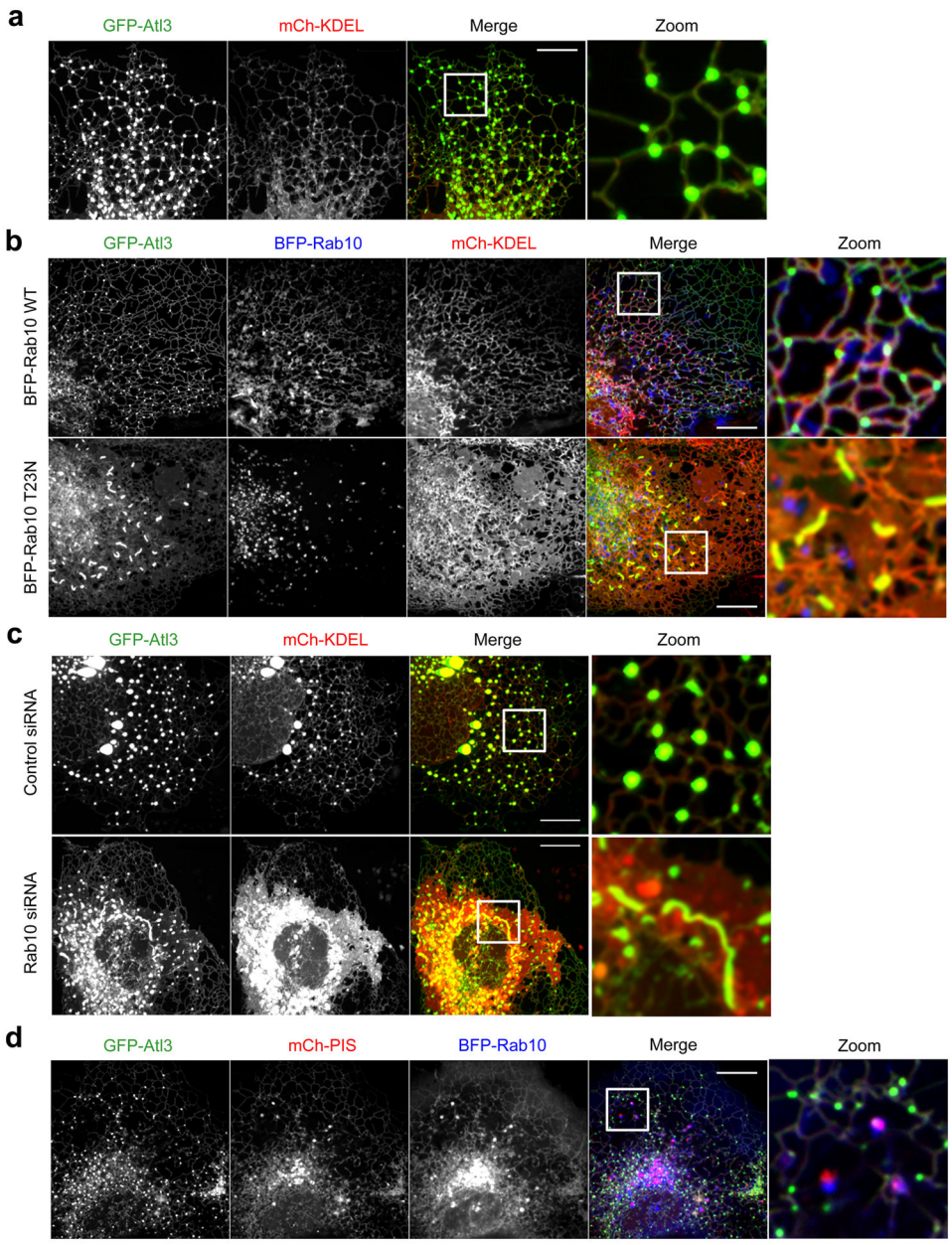

Figure 8. Atlastin and Rab10 do not overlap in function or location

a, Atl3 accumulates at 3-way junctions. Confocal images of Cos-7 cells co-expressing GFP-tagged human Atl3 (GFP-Atl3 in green) and an ER luminal marker (mCh-KDEL in red). **b,** Cos-7 cells expressing GFP-Atl3 (green) and mCh-KDEL (red) with BFP-Rab10 (blue) WT (top panel) or BFP-Rab10 T23N (bottom panel). Note that expansion of cisternal ER induced by Rab10 T23N expression, even in the presence of Atl3. **c,** Cos-7 cells were co-transfected with GFP-Atl3 (green), mCh-KDEL (red) and either control or Rab10 siRNA, note the expansive cisternae in the Rab10 siRNA depleted sample, even in the presence of Atl3. **d,** Live images of Cos-7 cells expressing GFP-Atl3 (green), mCh-PIS (red), and BFP-Rab10 WT (blue). Note that Atl3 puncta do not co-localize with Rab10/PIS puncta. For all

images: the second to last images shows merged images. The last panels show zoomed images of boxed regions in merge. Images in **a**, **b**, **c** and **d**, scale bars = 10 μm.